BMB
Reports

BMB Rep. 2018; 51(5): 236-241
www.bmbreports.org

Functional roles of glutamic acid E143 and E705 residues in the N-terminus and transmembrane domain 7 of Anoctamin 1 in calcium and noxious heat sensing

Jonghyun Choi[1,#], Yongwoo Jang[2,#], Haedong Kim[1], Jungwon Wee[3], Sinyoung Cho[1], Woo Sung Son[1], Sung Min Kim[4,5,] & Young Duk Yang[1,*]*

[1]College of Pharmacy, CHA University, Sungnam 13488, Korea, [2]Department of Psychiatry, McLean Hospital, Harvard Medical School, Belmont, MA 02478, USA, [3]Department of Molecular Medicine and Biopharmaceutical Sciences, Graduate School of Convergence Science and Technology, Seoul National University, Seoul 08826, [4]Department of Physical Education, College of Performing Arts and Sport, Hanyang University, Seoul 04763, [5]Department of Active Aging Industry, Graduate School, Hanyang University, Seoul 04763, Korea

Anoctamin 1 (ANO1) is an anion channel that is activated by changes in cytosolic Ca^{2+} concentration and noxious heat. Although the critical roles of ANO1 have been elucidated in various cell types, the control of its gating mechanisms by Ca^{2+} and heat remain more elusive. To investigate critical amino acid residues for modulation of Ca^{2+} and heat sensing, we constructed a randomized mutant library for *ANO1*. Among 695 random mutants, reduced Ca^{2+} sensitivity was observed in two mutants (mutant 84 and 87). Consequently, the E143A mutant showed reduced sensitivity to Ca^{2+} but not to high temperatures, whereas the E705V mutant exhibited reduced sensitivity to both Ca^{2+} and noxious heat. These results suggest that the glutamic acids (E) at 143 and 705 residues in ANO1 are critical for modulation of Ca^{2+} and/or heat responses. Furthermore, these findings help to provide a better understanding of the Ca^{2+}-mediated activation and heat-sensing mechanism of ANO1. [BMB Reports 2018; 51(5): 236-241]

INTRODUCTION

Intracellular Ca^{2+} and cAMP play an important role in the activation of chloride anion channels as second messengers (1, 2). In general, cAMP-activated chloride currents are mainly mediated by cystic fibrosis transmembrane conductance regulator (CFTR), an anion channel belonging to the ATP-binding cassette transporter gene family, whereas Ca^{2+}-activated chloride currents are mostly provided by Anoctamin 1 (ANO1, TMEM16A), an anion channel present in various cell types, including secretary epithelia cells, smooth muscle cells, and sensory neurons (3-5). Although it is clear that ANO1 is directly activated by Ca^{2+}, the molecular mechanisms that underlie Ca^{2+} gating remain elusive.

In 2008, ANO1 was identified as an integral membrane protein that contains 8 transmembrane-spanning helices with a cytosolic N- and C-terminus (6). In the absence of Ca^{2+}, ANO1 has also been shown to be gated by voltage (7). Moreover, ANO1 is activated by temperatures over 44°C, with strong heat sensitivity in sensory neurons (8). Since ANO1 is a Ca^{2+}-activated chloride channel, the gating mechanisms and binding modality of Ca^{2+} have been proposed by several studies. For instance, deletion of $_{448}$EAVK residues in the first intracellular loop of ANO1 leads to a reduced Ca^{2+} response (7). Amino acids $_{444}$EEEE are important for intrinsic voltage dependence, but mutating these residues has no effect on Ca^{2+} sensitivity (7). Moreover, Lee and colleagues suggested that two helices in the third intracellular loop could be structurally changed in a Ca^{2+}-dependent push-and-pull fashion, like a Ca^{2+} sensor (9). Because Ca^{2+} is a positively-charged ion, Tien and colleagues performed systematic mutagenesis of all conserved acidic residues in ANO1 (10). They determined that four putative acidic amino acids, E650, E698, E701, and E730, are defective in Ca^{2+}-induced ANO1 activation (10). Based on epitope and cysteine-scanning accessibility, revised topology of ANO1 described the fourth extracellular loop to be intracellular, and may include a Ca^{2+} binding site (11). Recently, the crystal structure of the fungal *Nectria haematococca* TMEM16 homologue was shown to be a phospholipid scramblase with 10 transmembrane domains and Ca^{2+}-dependent binding capability (12). The crystal

*Corresponding authors. Sung Min Kim, Tel: +82-2-2220-2880; Fax: +82-2-2220-1337; E-mail: minarthur@hanyang.ac.kr; Young Duk Yang, Tel: +82-31-881-7170; Fax: +82-31-881-7219; E-mail: ntsky0816@cha.ac.kr
#These authors contributed equally to this work.

https://doi.org/10.5483/BMBRep.2018.51.5.199

Received 20 October 2017, Revised 23 November 2017, Accepted 5 January 2018

Keywords: Anoctamin 1, Calcium sensitivity, Heat sensitivity, Random mutation

ISSN: 1976-670X (electronic edition)

structure revealed that the Ca^{2+} binding cavity is surrounded by three glutamates, two aspartates, and an asparagine located on alpha-helix 6, 7 and 8 (12). The function of fungal TMEM16 channels differs considerably from the typical features of ANO1 (6, 13, 14). Based on the determined Ca^{2+} binding domain (12), it is unclear how intracellular Ca^{2+} is able to move into its binding domain, which is deeply embedded inside lipid bilayer. Therefore, the Ca^{2+} binding residues and/or modulatory residues of mammalian ANO1 must be clarified. In the present study, we used error-prone PCR to generate random mutants, with the goal of identifying residues that are required for sensing Ca^{2+} and noxious heat.

RESULTS

High-throughput screening for random mutants in *ANO1* that affect Ca^{2+} response

To identify Ca^{2+}-binding residues and/or modulatory residues in ANO1, we set out to find putative residues from random mutants in mouse ANO1 (mANO1), ensuring an unbiased view on topology. First, we generated a stable cell line that expressed a halide-sensitive YFP (F46L/H148Q/I152L) construct in HEK293T cells for a high-throughput assay (Fig. 1A). Because the fluorescence emitted by the halide-sensitive YFP represents the concentration of cytosolic iodide, iodide influx induced by ANO1 activation leads to a decrease in fluorescence intensity (15, 16). To induce an increase in intracellular Ca^{2+} levels, we utilized the Ca^{2+} ionophore, A23187, a mobile ion-carrier widely used to study Ca^{2+} dynamics (17, 18). As expected, treatment with A23187 (10 μM) caused a decline in the relative YFP fluorescence intensity (Fig. 1B).

Random mutations in *ANO1* were achieved using error-prone PCR, which generated 695 randomized ANO1 mutants. Using halide-sensitive YFP stable cell lines, we selected 14 candidates that showed a decreased response to Ca^{2+} (Fig. 1C). After more intense YFP imaging, we selected two promising candidates, mutant 84 and mutant 87, whose response to Ca^{2+} was almost abolished. As shown in Fig. 1D and E, A23187 treatment robustly reduced the intensity of YFP fluorescence in WT ANO1-transfected YFP stable cells, whereas mutant 84- and 87-transfected YFP stable cells showed significantly lower responses to Ca^{2+} (Fig. 1D and E).

Response of E143A and E705V ANO1 mutants to Ca^{2+} and noxious heat

To identify the mutated residues in mutants 84 and 87, we performed further sequencing analysis. We found several mutations in the amino acid sequence of mouse ANO1 (E143A, L191M, P721H, and E943V in mutant 84; E705V in mutant 87) (Fig. 2A). Each single point mutation in *ANO1* was constructed from the mutation results above, and we investigated differences in the Ca^{2+} response between WT and each single mutant using YFP imaging. From this, we were able to rule out L191M, P721H, and E943V mutants because they

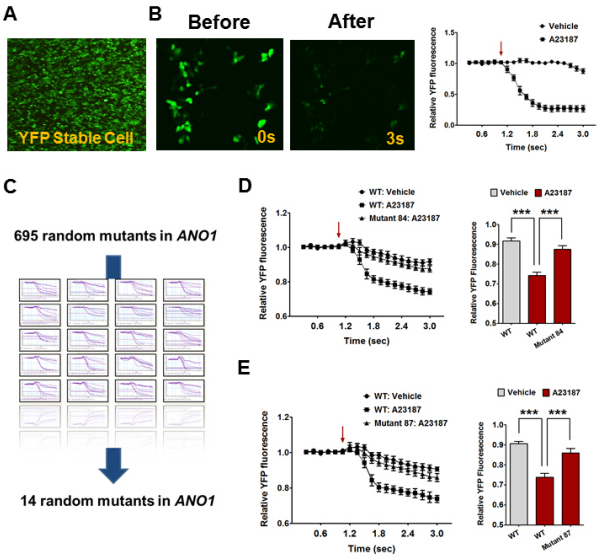

Fig. 1. High throughput screening for random mutants in *ANO1* responding to Ca^{2+}. (A) The YFP fluorescence emitted from the halide-sensitive YFP stable HEK293T cells. Arrow indicates an injection point of vehicle or A23187. (B) The treatment of A23187 (10 μM) cause the decline in relative YFP fluorescence intensity in YFP stable HEK293T cells. (C) The schematic process for ANO1 mutants screening assay. 14 random mutants were screened from the 695 mutants library. (D) Mutant 84 shows significantly a reduced sensitivity to A23187 compared with wild-type (WT) ANO1. ***P < 0.001, Arrow indicates an injection point of vehicle or A23187. (E) Mutant 87 shows significantly a reduced sensitivity to A23187 compared with WT ANO1. ***P < 0.001, Arrow indicates an injection point of vehicle or A23187.

showed no significant difference in Ca^{2+}-induced ANO1 activation (Supplementary Fig. 1). However, both E143A and E705V mutants showed a significantly lower response to A23187-induced ANO1 activation compared to WT (Fig. 2C and D). Indeed, alignments of all ANOs revealed that the E705 residue in *ANO1* was broadly conserved across the ANO family, whereas the E143 residue was found only in ANO1 to 6 (Fig. 2B).

ANO1 is also known to be activated by noxious heat (above 44°C) (8). Thus, we wondered whether these mutations could also affect the heat-sensing ability of ANO1. As shown in Fig. 2E, the E143A ANO1 mutant showed a similar response as WT to heat stimulus (44°C), whereas the E705V ANO1 mutant exhibited a significantly lower response to noxious heat compared to WT (Fig. 2F). Moreover, L191M, P721H, and E943V mutants also showed no significant difference in heat-induced ANO1 activation (Supplementary Fig. 2A-C).

It is possible that these mutants could alter the proper targeting of ANO1 to the plasma membrane, which would result in impaired channel activity or sensitivity. Thus, we determined mRNA and protein expression levels in WT cells, and E143A and E705V mutants. Reverse transcription PCR

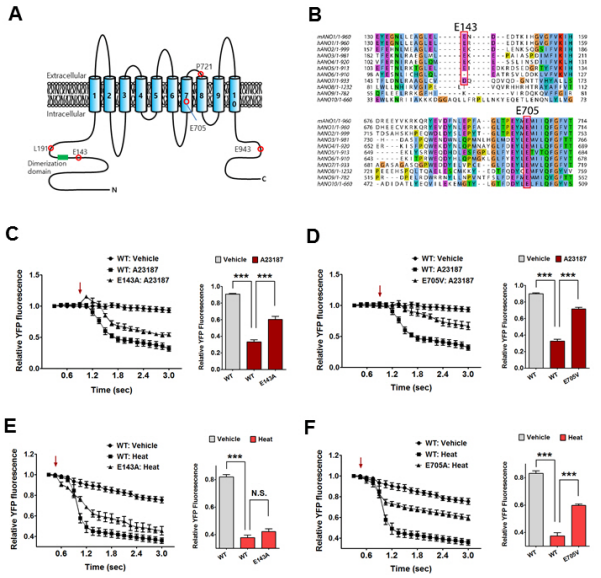

Fig. 2. The response of E143A and E705V ANO1 mutants to Ca^{2+} and noxious heat. (A) Topological model of mouse ANO1. E143 residue is located in the N-terminus of ANO1, and E705V is located in a fourth intracellular loop of ANO1. (B) Multiple alignments among ANO family. E143 residue is widely conserved in other ANOs except for ANO7, ANO8, ANO9, and ANO10. Meanwhile E705 residue is widely conserved among all ANOs. (C) E143A ANO1 mutant shows significantly a reduced sensitivity to A23187 compared with WT ANO1. ***P < 0.001, Arrow indicates an injection point of vehicle or A23187. (D) E705V ANO1 mutant shows significantly a reduced sensitivity to A23187 compared with WT ANO1. ***P < 0.001, Arrow indicates an injection point of vehicle or A23187. (E) There is no difference in the heat sensitivity between WT and E143A ANO1 mutant. Arrow indicates an injection point of vehicle or heat (44°C). (F) E705V ANO1 mutant shows significantly a reduced sensitivity to noxious heat (44°C) compared with WT ANO1. ***P < 0.001, Arrow indicates an injection point of vehicle or heat (44°C).

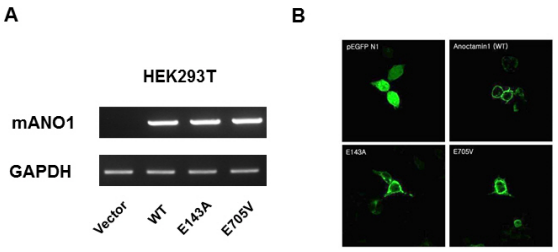

Fig. 3. mRNA levels and localization of WT and mutant ANO1. (A) There is no difference in the mRNA levels among WT, E143A, and E705V ANO1. (B) GFP-tagged WT, E143A, and E705V ANO1 are normally observed in the plasma membrane.

(RT-PCR) analysis of WT-, E143A-, and E705V ANO1-transfected cells showed normal transcriptional expression in the mutant cells (Fig. 3A). To monitor protein expression and localization, we constructed green fluorescence protein (GFP)-tagged WT and mutant proteins. Transfection of these plasmids into HEK293T cells showed normal localization to the plasma membrane in both mutant cell lines (Fig. 3B). These results suggest that glutamic acids at 143 and 705 residues of ANO1 play a crucial role in sensing intracellular Ca^{2+}. Moreover, the E705 residue is also involved in the heat sensitivity of ANO1.

Role of the glutamic acid 143 residue in the N-terminus of ANO1 in dimer formation

According to previous reports, the cytosolic N-terminus of ANO1 is important for dimer formation (19, 20). Thus, we investigated whether the E143 residue in the N-terminus of ANO1 is involved in dimer formation. To this end, we determined protein interactions in the E143A mutant using a bimolecular fluorescence complementation technique known as BiFC (21, 22). Upon interaction or close spatial proximity, two protein fragments (VC155 and VN173) of YFP assemble and enhance the YFP fluorescence intensity (21, 22). Therefore, we incorporated WT and mutant E143A into the VC155 and VN173 constructs, respectively. As shown in Fig. 4, either the VC155-WT ANO1 or VN173-WT ANO1 construct alone failed to emit YFP fluorescence, but overexpression of both WT ANO1-VC155 and WT ANO1-VN173 successfully emitted YFP fluorescence. Enhanced YFP fluorescence was observed around the plasma membrane, indicating dimeric translocation of ANO1 towards the plasma membrane. Meanwhile, a normal interaction between E143A-VC155 and E143A-VN173 was also observed, similar to WT ANO1, suggesting that the mutation at glutamic acid 143 residue in the N-terminus of ANO1 does not affect dimerization. From the investigation of electrostatic surface potential of mouse ANO1, the amino acids around 143E exposed to intercellular space were identified to be negatively charged. Therefore, the negatively charged region (121E-150I) was chosen and further generated a deletion mutant at residues 121 to 150, where acidic amino acids (E and D) are repeatedly arranged at the N-terminus (Fig. 4B). This deletion mutant (Δ 121-150) showed normal localization to the plasma membrane, similar to WT ANO1. Surprisingly, the Ca^{2+} sensitivity of ANO1 totally disappeared in the Δ 121-150 mutant (Fig. 4C). These results seem to be related to the charge properties of the residues of protein adjacent to membrane. In fact, a three-dimensional structure supported that when the large negative charge region containing E143 is cleaved, the positively charged calcium ions appear to be more difficult to approach truncated protein than the wild type of mouse ANO1 (Fig. 4C). However, the Δ 121-150 mutant showed no significant difference in heat-induced ANO1 activation (Supplementary Fig. 2D). Taken together, the negative charge of E143 residue in N-terminus helps the calcium ions to move into its binding domain of ANO1.

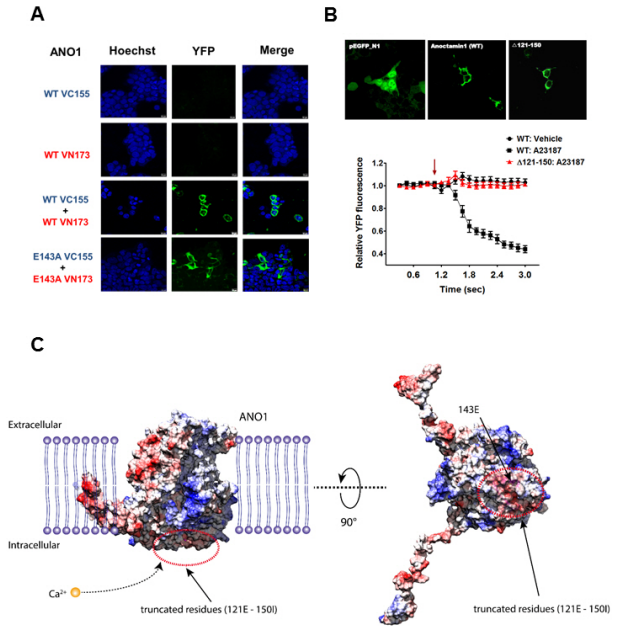

Fig. 4. The E143 residue of the N-terminus of ANO1 on dimer formation. (A) Alone VC155 or VN173 construct fails to emit YFP fluorescence (first and second row images). However, co-overexpression of VC155 and VN173 emits the YFP fluorescence (pBiFC-VC155 and VN173 was a gift from Chang-Deng Hu, Addgene, third row images). When WT ANO1-VC155 and WT ANO1-VN173 were co-overexpressed, the YFP signals are observed around plasma membrane (forth row images). Moreover, co-overexpression of E143A ANO1-VC155 and E143A ANO1-VN173 emits the YFP fluorescence signals around plasma membrane (fifth row images). (B) GFP-tagged WT and ANO1 mutant (Δ 121-150) are normally observed in the plasma membrane (Upper). The A23187-induced ANO1 activation is disappeared in the ANO1 deletion mutant (Lower). Arrow indicates an injection point of vehicle or A23187. (C) The electrostatic surface potential (ESP) of mouse ANO1 structure are represented by red (negatively charged) and blue (positively charged) color, respectively. Energy scale is from -10 to 10 in units of kcal/(mole*e). Secondary structure of truncated region is colored by magenta and 143E residue at truncated region is colored by yellow, respectively.

DISCUSSION

The Ca^{2+}-activated chloride channel, ANO1 is an important player in numerous physiological functions such as ion transport, fluid secretion, smooth muscle contraction, neuronal excitability, and cell proliferation (3, 23, 24). Although the critical roles of ANO1 have been elucidated in various cell types, the binding domain and Ca^{2+} gating mechanism of ANO1 are still elusive. The present study used randomized mutagenesis of *ANO1*, without a biased view on topology, to identify putative residues of ANO1 that may be involved in Ca^{2+} and noxious heat sensing.

Among the 695 randomly-generated *ANO1* mutants, we identified two critical residues, E143 in the N-terminus and E705 in the fourth loop of ANO1 that are critical for Ca^{2+} sensitivity. Interestingly, positively-charged Ca^{2+} has a binding tendency for carboxylate moieties of acidic amino acid residues such as glutamic acid and aspartic acid (25). Thus, we investigated the effects of the glutamic acids at 143 and 705 residues on Ca^{2+} binding to ANO1.

The N-terminus of ANO1, including the E143 residue, is known to regulate membrane trafficking and protein interactions for dimerization (19, 20, 26). Analysis of the expression pattern of E143A-GFP showed some GFP signal beneath the plasma membrane, but it appeared to be generally localized on the plasma membrane (Fig. 3). Regarding its potential role in dimerization of ANO1, we performed a BiFC technique, and like WT, a normal interaction was found between E143A-VC155 and E143A-VN173 (Fig. 4). Therefore, it seems that the E143 residue in the N-terminus of ANO1 is not involved in membrane trafficking or protein interactions. According to Tien and colleagues, the E143A mutation has no effect on Ca^{2+}-sensitivity, from inside-out excised patch data (10). However, in the present study, we found reduced activity to Ca^{2+} in the whole cell mode using a YFP imaging system, suggesting that the E143 residue could be involved in indirect regulation of Ca^{2+} sensitivity, through Ca^{2+}-mediated modulators such as calmodulin (27). In fact, the N-terminus of ANO1 is known to physically interact with calmodulin (23). Thus, it is possible to modulate the Ca^{2+} binding residue through the co-interaction with calmodulin. As shown in Fig. 4C, a three-dimensional structure suggest that the negative charges in the N-terminus of ANO1 might help positive charged Ca^{2+} ions to trap within membrane boundary as a Ca^{2+} reservoir. Therefore, the capture of Ca^{2+} ions in the N-terminus might be important first step to move into Ca^{2+} binding site in membrane plasma. Indeed, molecular modeling supported that the deletion of large negative charge region containing E143 causes charged calcium ions to be more difficult to approach truncated protein than the wild type of ANO1 (Fig. 4C). Therefore, these results suggest that the acidic amino acid-rich region at the N-terminus coordinates with Ca^{2+} and control activation by Ca^{2+}.

According to first definition of ANO1 topology, the E705 residue was reported to be in the extracellular fourth loop, but a recent study showed that it is actually in an intracellular loop (11). Yu and colleagues showed that the fourth loop includes acidic E702 and E705 residues that act as calcium binding sites. Based on the fungal ANO1 crystal structure, it was proposed that the Ca^{2+} binding moiety of fungal ANO1 is highly conserved with several amino acids in the fourth loop of mouse ANO1 (12). Consistent with this, the current study demonstrated that the E705V mutant showed a severe defect in Ca^{2+} sensitivity compared with WT ANO1 (Fig. 2). In addition, we further demonstrated that the mutation in the E705 residue strongly reduced its sensitivity to noxious heat (Fig. 2). Considering that the heat-mediated gating mechanism of ANO1 still unclear, the fourth loop, including the E705

residue, may also be capable of sensing temperature.

In summary, our randomized mutagenesis approach identified two glutamic acids at E143 and E705 residues of ANO1, which are critical for Ca^{2+}-sensing. The E143 residue in the N-terminus regulates Ca^{2+} sensitivity, but is not involved in temperature-mediated activation. Meanwhile, the E705 residue in the fourth intracellular loop strongly affects the Ca^{2+}- and heat-sensitivity of ANO1. In particular, we propose an important role for the E705 residue in heat-mediated ANO1 gating.

MATERIALS AND METHODS

Cell culture and transfection

Stable cells were grown in Dulbecco's Modified Eagle Medium containing 4.5 $mg.ml^{-1}$ glucose, 10% fetal bovine serum (FBS), 50 $units.ml^{-1}$ penicillin and 50 $ug.ml^{-1}$ streptomycin. Cells were cultured in a 37°C humidified incubator of 95% O_2 and 5% CO_2. Cells were transfected using Lipofectamin 2000 (Invitrogen, Carlsbad, California) according to the manufacturer's instructions.

Generation of halide sensitive-YFP stable cell line

HEK293T-FRT cells were co-transfected with pcDNA5/FRT (Invitrogen) vector containing YFP-H148Q/I152L (friendly gifted from Prof. Wan Namkung, Yonsei University, Incheon, Korea) and pOG44 (Flp recombinase expression) using Lipofectamin 2000. Transfected cells were selected with positive selection marker, hygromycin B.

Generation of mutant library

Three sets of error-prone PCR (Diversify PCR random mutagenesis kit, Clontech, Mountain View, CA) were performed on mouse *ANO1*. In the first round, error-prone PCR was performed on the entire gene using forward and reverse primers to sequences outside the open reading frame. According to manufacturer's protocol, mutation rates of 2 mutations/kb were chosen. These fragments were ligated into the pcDNA5-FRT mammalian expression vector using In-Fusion® HD Cloning Kit (Clontech).

Halide sensitive YFP imaging

HEK293T-YFP cells were plated in 96 well black clear bottom plates at approximately 10,000 cells per well. After 24 hours, WT ANO1 or mutants ANO1 was transfected using Lipofectamin 2000 (Invitrogen) according to the manufacturer's instructions. YFP fluorescence intensity was measured 48hr later with two different stimulations, Ca^{2+} and high temperature. To measure fluorescent intensity responding to Ca^{2+}, the cells were washed two times with phosphate buffer solution (PBS, pH 7.4), and then incubated with modified NaCl solution (in mM: 140 NaCl, 10 HEPES, 10 glucose, 5 KCl, 1 $MgCl_2$ and 1 $CaCl_2$, pH 7.4) in 37°C, 5% CO_2 incubator for 30 min. After incubation, the fluorescence intensity was continuously acquired per 0.15 sec for total 3 sec using Flex station 2 (Molecular Devices, Sunnyvale, California). The 10 μM A23187 in NaI solution (in mM: 140 NaI, 10 HEPES, 10 glucose, 5 KCl, 1 $MgCl_2$ and 1 $CaCl_2$, pH 7.4) injected on the cells at 0.90 or 1.05 sec by injector cartridge module with Flex station 2. For measure heat response to ANO1, the fluorescence intensity was continuously acquired per 0.15 sec for total 3 sec on SpectraMax® i3x microplate reader. The NaI solution controlled 44°C was promptly exposed to the cells at 0.45 or 0.90 sec using with the SpectraMax® i3x injector module.

Site-directed Mutagenesis

ANO1 mutants and GFP tagged constructs were generated using the site-directed mutagenesis kit (iNtRON Biotech, South Korea) according to the manufacturer's instruction. Mutation in the desired amino acids of mANO1 were generated by substitution of the central 1-2 nucleotides with two complimentary of mutagenic primers, respectively. PCR-based site-directed mutagenesis was performed using T100 thermal cycler (Bio Rad, 95°C for 30 sec, then 95°C for 30 sec, 55°C for 1 min, 68°C for 6 min at 15-18 cycles). Mutants were verified by sequencing.

Generation of green fluorescent protein (GFP) tagging

The mANO1 coding sequence was incorporated into pEGFPN1 vector which is tagged GFP on the C-terminal region. The stop codon of ANO1 deleted for continuously initiating the translation of GFP.

Reverse transcription PCR (RT-PCR)

Total RNA was extracted using easy-BLUE™ solution (iNtRON Biotech), and reverse transcribed using a First Strand cDNA Synthesis Kit (Roche Applied Science). RT-PCR was performed as per the manufacturer's instructions using sets of specific primers, namely forward (5′ CTTCAAAGGCCGGTTTGTTGG 3′) and reverse (5′ TTGACGAAGCCGTGCATGGTC 3′).

Three dimensional structure of ANO1

Three-dimensional structure of mouse ANO1 was obtained using I-TASSER (28) method with template X-ray crystal structure (4WIS). The electrostatic surface potentials (ESP) of mouse ANO1 structure were calculated and investigated utilizing Coulombic surface coloring method in UCSF Chimera (29). Also, molecular visualization of structure was presented with UCSF Chimera.

Statistics

All results are shown as means ± SEMs. The one-way ANOVA was used to conduct multiple comparisons of means. Statistical significance was accepted for P values of < 0.05 (*), 0.01 (**), or 0.001 (***).

ACKNOWLEDGEMENTS

This research was supported by a grant from the National Research Foundation (NRF) of Korea (NRF-2015R1C1A1A 02037682, Y Yang). Also, this work was partly supported by the GRRC program of Gyeonggi province (GRRC-CHA2017-A02, Validity and Safety Evaluation of Regional Specialized Resources).

CONFLICTS OF INTEREST

The authors have no conflicting interests.

REFERENCES

1. Begenisich T and Melvin JE (1998) Regulation of chloride channels in secretory epithelia. J Membr Biol 163, 77-85
2. Kunzelmann K and Mehta A (2013) CFTR: a hub for kinases and crosstalk of cAMP and Ca2+. FEBS J 280, 4417-4429
3. Jang Y and Oh U (2014) Anoctamin 1 in secretory epithelia. Cell Calcium 55, 355-361
4. Oh U and Jung J (2016) Cellular functions of TMEM16/anoctamin. Pflugers Arch 468, 443-453
5. Ha GE and Cheong E (2017) Calcium-activated chloride channels: a new target to control the spiking pattern of neurons. BMB Rep 50, 109-110
6. Yang YD, Cho H, Koo JY et al (2008) TMEM16A confers receptor-activated calcium-dependent chloride conductance. Nature 455, 1210-1215
7. Xiao Q, Yu K, Perez-Cornejo P, Cui Y, Arreola J and Hartzell HC (2011) Voltage- and calcium-dependent gating of TMEM16A/Ano1 chloride channels are physically coupled by the first intracellular loop. Proc Natl Acad Sci U S A 108, 8891-8896
8. Cho H, Yang YD, Lee J et al (2012) The calcium-activated chloride channel anoctamin 1 acts as a heat sensor in nociceptive neurons. Nat Neurosci 15, 1015-1021
9. Lee J, Jung J, Tak MH et al (2015) Two helices in the third intracellular loop determine anoctamin 1 (TMEM16A) activation by calcium. Pflugers Arch 467, 1677-1687
10. Tien J, Peters CJ, Wong XM et al (2014) A comprehensive search for calcium binding sites critical for TMEM16A calcium-activated chloride channel activity. Elife 3
11. Yu K, Duran C, Qu Z, Cui YY and Hartzell HC (2012) Explaining calcium-dependent gating of anoctamin-1 chloride channels requires a revised topology. Circ Res 110, 990-999
12. Brunner JD, Lim NK, Schenck S, Duerst A and Dutzler R (2014) X-ray structure of a calcium-activated TMEM16 lipid scramblase. Nature 516, 207-212
13. Caputo A, Caci E, Ferrera L et al (2008) TMEM16A, a membrane protein associated with calcium-dependent chloride channel activity. Science 322, 590-594
14. Schroeder BC, Cheng T, Jan YN and Jan LY (2008) Expression cloning of TMEM16A as a calcium-activated chloride channel subunit. Cell 134, 1019-1029
15. Zhong S, Navaratnam D and Santos-Sacchi J (2014) A genetically-encoded YFP sensor with enhanced chloride sensitivity, photostability and reduced ph interference demonstrates augmented transmembrane chloride movement by gerbil prestin (SLC26a5). PLoS One 9, e99095
16. Namkung W, Thiagarajah JR, Phuan PW and Verkman AS (2010) Inhibition of Ca2+-activated Cl- channels by gallotannins as a possible molecular basis for health benefits of red wine and green tea. FASEB J 24, 4178-4186
17. Cho Y, Jang Y, Yang YD, Lee CH, Lee Y and Oh U (2010) TRPM8 mediates cold and menthol allergies associated with mast cell activation. Cell Calcium 48, 202-208
18. Dewitt S, Laffafian I, Morris MR and Hallett MB (2003) Cytosolic Ca2+ measurement and imaging in inflammatory cells. Methods Mol Biol 225, 47-59
19. Scudieri P, Musante I, Gianotti A, Moran O and Galietta LJ (2016) Intermolecular Interactions in the TMEM16A Dimer Controlling Channel Activity. Sci Rep 6, 38788
20. Tien J, Lee HY, Minor DL Jr, Jan YN and Jan LY (2013) Identification of a dimerization domain in the TMEM16A calcium-activated chloride channel (CaCC). Proc Natl Acad Sci U S A 110, 6352-6357
21. Lonn P and Landegren U (2017) Close Encounters - Probing Proximal Proteins in Live or Fixed Cells. Trends Biochem Sci 42, 504-515
22. Miller KE, Kim Y, Huh WK and Park HO (2015) Bimolecular Fluorescence Complementation (BiFC) Analysis: Advances and Recent Applications for Genome-Wide Interaction Studies. J Mol Biol 427, 2039-2055
23. Jung J, Nam JH, Park HW, Oh U, Yoon JH and Lee MG (2013) Dynamic modulation of ANO1/TMEM16A HCO3(-) permeability by Ca2+/calmodulin. Proc Natl Acad Sci U S A 110, 360-365
24. Cho H and Oh U (2013) Anoctamin 1 mediates thermal pain as a heat sensor. Curr Neuropharmacol 11, 641-651
25. Pidcock E and Moore GR (2001) Structural characteristics of protein binding sites for calcium and lanthanide ions. J Biol Inorg Chem 6, 479-489
26. Suzuki T, Suzuki J and Nagata S (2014) Functional swapping between transmembrane proteins TMEM16A and TMEM16F. J Biol Chem 289, 7438-7447
27. Pedemonte N and Galietta LJ (2014) Structure and function of TMEM16 proteins (anoctamins). Physiol Rev 94, 419-459
28. Zhang Y (2008) I-TASSER server for protein 3D structure prediction. BMC bioinformatics 9, 40
29. Pettersen EF, Goddard TD, Huang CC et al (2004) UCSF Chimera--a visualization system for exploratory research and analysis. J Comput Chem 25, 1605-1612